HRSC on Mars Express – Photogrammetric and Cartographic Research

Joerg Albertz, Maria Attwenger, Janet Barrett, Simon Casley, Peter Dorninger, Egon Dorrer, Heinrich Ebner, Stephan Gehrke, Bernd Giese, Klaus Gwinner, Christian Heipke, Elpitha Howington-Kraus, Randolph L.Kirk, Hartmut Lehmann, Helmut Mayer, Jan-Peter Muller, Juergen Oberst, Alexey Ostrovskiy, Joerg Renter, Sergiy Reznik, Ralph Schmidt, Frank Scholten, Michael Spiegel, Uwe Stilla, Marita Wählisch, Gerhard Neukum, and the HRSC Col-Team.

Abstract

The High Resolution Stereo Camera (HRSC) on the European spacecraft Mars Express is the first camera on a planetary mission especially designed for photogrammetric and cartographic purposes. Since January 2004 the camera has been taking image data from the Martian surface, characterized by high-resolution, stereo capability and color. These data provide an enormous potential for the generation of 3D surface models, color orthoimages, topographic and thematic maps, and additional products. The image data acquired undergo calibration and systematic processing to orthoimages and 3D data products. Within the international HRSC Science Team the members of the Photogrammetric/Cartographic Working Group are concerned with further refinements in order to achieve highest quality data products. These activities comprise improvements of the exterior orientation of the camera, various approaches to enhance DTM quality, and the generation of maps in the standard scale of 1:200 000 and larger scales as well. The paper reports on these activities and the results achieved so far.

Introduction

The High Resolution Stereo Camera (HRSC) is part of the orbiter payload on the ESA mission *Mars Express* (MEX). For the first time in planetary exploration, a camera system has especially been designed to meet the requirements of photogrammetry and cartography for mapping the complete surface of a planet. For this purpose HRSC operates as a pushbroom scanning instrument with nine CCD line detectors mounted in parallel in the focal plane of the camera. Data acquisition is achieved in five panchromatic channels under different observation angles and four color channels (for details see Neukum *et al.*, 2004). Thus, the data provided are well-suited for the generation of Digital Terrain Models (DTMs) and other 3D data products by stereo photogrammetric evaluation, the derivation of orthoimage mosaics in color, and the compilation of Topographic Image Maps. These products close the gap between medium- to low-resolution imagery and very high-resolution data available from parts of the Martian surface from previous missions. In addition, the Super Resolution Channel (SRC) of HRSC, a framing camera, provides still higher resolution images from small segments of the Martian surface.

Under the guidance of Gerhard Neukum, the Principal Investigator (PI), the HRSC experiment is organized into several teams. More than 40 Co-Investigators (COIS) form the international Science Team, which is subdivided into working groups by discipline. These working groups are devoted to geoscience, photogrammetry/cartography, spectrophotometry, and atmospheric science. The members of the Photogrammetric/Cartographic Working Group (PCWG) have joined efforts to improve photogrammetric and cartographic products, and thus serve the scientific community as best as they can.

Since January 2004 the camera has been imaging the Martian surface, and provides image data with a maximum

J. Albertz, S. Gehrke, and H. Lehmann are with the Institute for Geodesy and Geoinformatics, Technical University Berlin, H 12, Str. des 17. Juni 135, D-10623 Berlin, Germany (albertz@fpk.tu-berlin.de).

M. Attwenger and P. Dorninger are with the Institute of Photogrammetry and Remote Sensing, Vienna University of Technology, Gusshausstr. 27–29, A-1040 Wien, Austria (kk@ipf.tuwien.ac.at).

J. Barrett, E. Howington-Kraus, and R. Kirk are with the Astrogeology Team, U.S. Geological Survey, 2255 N. Gemini Dr., Flagstaff, AZ 86001 USA (rkirk@usgs.gov).

S. Casley and J. Muller are with the University College London, Department of Geomatic Engineering, Gower Str., London WC1E 6BT, UK (jpmuller@ge.ucl.ac.uk).

E. Dorrer, H. Mayer, A. Ostrovskiy, J. Renter, and S. Reznik are with the Institute for Photogrammetry and Cartography, Munich Bundeswehr University, Werner-Heisenberg-Weg 35, D-85577 Neubiberg, Germany (egon.dorrer@unibw-muenchen.de).

H. Ebner, M. Spiegel, and U. Stilla are with the Technical University Munich, Photogrammetry and Remote Sensing, Arcisstr. 21, D-80333 München, Germany (stilla@bv.tum.de).

B. Giese, K. Gwinner, J. Oberst, F. Scholten and M. Wählisch are with the German Aerospace Center (DLR), Institute of Planetary Research, Rutherfordstr. 2, D-12489 Berlin, Germany (juergen.oberst@dlr.de).

C. Heipke and R. Schmidt are with the Institute of Photogrammetry and GeoInformation, University of Hannover, Nienburger Str. 1, D-30167 Hannover, Germany (heipke@ipi.uni-hannover.de).

G. Neukum is with the Freie Universität Berlin, Institute of Geological Sciences/Planetology, Malteserstr. 74–100, D-12249, Berlin, Germany (gneukum@zedat.fu-berlin.de).

Photogrammetric Engineering & Remote Sensing
Vol. 71, No. 10, October 2005, pp. 1153–1166.

0099-1112/05/7110–1153/$3.00/0

resolution of approximately 10 m. Calibration and systematic processing of the data are carried out by the Institute of Planetary Research of the German Aerospace Center (DLR), as described by Scholten *et al.* (2005). It is self-evident that a great variety of effects influence the accuracy and the quality of the 3D products, the orthoimages, and the topographic and thematic maps. Therefore, the members of the PCWG have developed various approaches to achieve highest quality results by the application of sophisticated processing techniques. This also comprises the integration of existing data, especially the results of the Mars Orbiter Laser Altimeter (MOLA). These data provide high accuracy and consistent control information and are therefore recommended and generally accepted as reference for mapping Mars (Neumann *et al.*, 2003).

In the following sections the PCWG members report about their activities. Despite the fact that the mission is still in its initial phase, impressive experiment results have already been obtained at the time of writing (October 2004). The topics encompass mainly three subjects, i.e., improvement of exterior orientation parameters for HRSC imagery, enhancement of the quality of the DTMs, and generation of topographic maps as a final result of the data processing stream. In particular, several contributors discuss different successful approaches that further improve the present routine DTM generation process with its restriction to intensity-based image matching. They range from stereo photogrammetric processing, elimination of measurement noise and modeling linear structures, point densification using adaptive least-squares correlation, to a shape-from-shading approach. All these investigations are based on the developments described in Scholten *et al.* (2005), i.e., systematically calibrated Level-2 data provided to the entire HRSC COI team, as well as standard Level-4 orthoimage and DTM products and specific data provided by DLR for the respective developments.

Improving the Exterior Orientation of Mars Express HRSC Imagery

The Flight Dynamics Team at ESOC use earth-based radiometric tracking data (Doppler and ranging) of the MEX spacecraft and telemetered data from the on-board star camera and gyros to compute the spacecraft orbit and attitude data. These measurements result in a three-dimensional spacecraft position and camera orientation (the camera alignment on the spacecraft is known) over time termed exterior orientation (EO) in classical photogrammetry. The interior orientation (IO) of the HRSC has been calibrated in a laboratory at Dornier, Friedrichshafen and has been verified during the six month journey to Mars by means of star observations. So far, no deviations from the calibration have been experienced so that the IO of the HRSC is considered to be stable. These values can be improved in their relative and absolute accuracy. This is accomplished in two steps. First, large numbers of tie points between the multiple stereo strips are extracted using digital image matching (DIM). Then, a photogrammetric bundle adjustment is performed to correct the EO, using the collected tie points as direct observations for the unknown EO parameters.

The absolute accuracy of the initial orbit data is at the 0.1 to 1.5 km level. The relative or internal consistency accuracy within an orbit is orders of magnitude more accurate. Here, ground control information is required to tie the orbit through the HRSC object points to the Mars-fixed coordinate system. We show an approach in which the absolute positioning of the HRSC points is achieved within the bundle adjustment procedure.

Matching

Our matching approach follows a coarse to fine resolution strategy, which means that the matching result is refined step by step through image pyramids. The HRSC imagery, the observed EO, and the calibration data of the interior orientation (IO) are needed as input.

At first, point features are extracted using the Förstner operator (Förstner, 1986); the images are matched pairwise in all combinations using the cross correlation coefficient as a similarity measure. Each image is divided into sub-areas to ensure an even distribution of the tie points over the whole area. To reduce ambiguities and computing time the matching location and a search space for the corresponding feature is computed when transferring a feature from one image to the other. Since no epipolar geometry exists for linescanner imagery, a feature in one image is transferred to the next image using Equation 1 (Ebner *et al.*, 1994):

$$\begin{pmatrix} x - x_0 \\ y - y_0 \\ -c \end{pmatrix} = \lambda M^T(\Delta\varphi,\Delta\omega,\Delta\kappa)\, D^T(\varphi,\omega,\kappa)\left[\begin{pmatrix} X \\ Y \\ Z \end{pmatrix} - \begin{pmatrix} X_0 + \Delta X_0 \\ Y_0 + \Delta Y_0 \\ Z_0 + \Delta Z_0 \end{pmatrix}\right] \quad (1)$$

For the transformation from object space to image space as a function of the image line (readout cycle) **n** an additional condition (Equation 2) has to be introduced where **x** points in the flight direction:

$$x(n) = x(n, X_0(n), Y_0(n), Z_0(n), \varphi(n), \omega(n), \kappa(n)) = 0 \quad (2)$$

This problem can be solved using the Newton-method for the above zero-crossing detection where the derivative $x'(n_i)$ is replaced by the pixel size of the image (Equation 3):

$$n_0 = \textit{initial value for the image line}$$
$$n_{i+1} = n_i - x(n_i)/\textit{pixelsize} \qquad i = 0,1,\ldots \quad (3)$$

The point tuples are generated by applying a Random Sample Consensus (RANSAC) procedure (Fischler and Bolles, 1981). From the start pyramid level (lowest resolution) to the so-called intermediate level (medium resolution), feature-based matching is carried out on the entire images. Going down the image pyramid, the image resolution and the number of extracted features increase. Besides the heavily increasing computational time, the matching of the complete images would result in an exceedingly large number of tie points. Therefore, the matching procedure is carried out only for selected "image chips", starting from the intermediate pyramid level. Tie points are searched for only in those areas where points have been found before.

To further refine the positional measurements of the tie points, Multi-Image Least Squares Matching (MILSM) is carried out. In our approach the tie points are matched simultaneously in all images (see Heipke *et al.*, 2004).

Finally, model points are derived using a forward intersection of the image coordinates of the tie points. They serve as an approximation for the reduction of the search space on the next lower pyramid level. In our implementation of the matching software, we also can use a Mars DTM (which will be discussed later) to find the approximate search area for points. A more detailed description of the application flow can be found in Schmidt and Brand (2003).

Bundle Adjustment

The mathematical model for photogrammetric point determination with a three-line camera is based on the collinearity Equation 1. Typically, we determine only constant offsets of

these parameters (Equation 4), though modeling of drifts is possible:

$$X_0 = \overline{X}_{B_0} + \overline{X}_0,\ Y_0 = \overline{Y}_{B_0} + \overline{Y}_0,\ Z_0 = \overline{Z}_{B_0} + \overline{Z}_0,$$
$$\varphi = \overline{\varphi}_B + \overline{\varphi},\ \omega = \overline{\omega}_B + \overline{\omega},\ \kappa = \overline{\kappa}_B + \overline{\kappa} \quad (4)$$

whereas the EO is composed of biases ($\overline{X}_{B_0}$, $\overline{Y}_{B_0}$, $\overline{Z}_{B_0}$, $\overline{\varphi}_B$, $\overline{\omega}_B$, $\overline{\kappa}_B$) valid for the entire strip, and the values ($\overline{X}_0$, $\overline{Y}_0$, $\overline{Z}_0$, $\overline{\varphi}$, $\overline{\omega}$, $\overline{\kappa}$) are the observed EO data per CCD line which are considered to be fixed and free of errors (see Müller, 1991). This solution keeps the number of orientation parameters small and allows us to take advantage of the good relative accuracy of the observed orientation parameters.

Tying HRSC to MOLA Data

While it is possible to derive internally consistent control point solutions, it is highly desirable to tie the HRSC control points to the Mars-fixed coordinate system. The MOLA DTM (Neumann *et al.*, 2003) is introduced into the bundle adjustment by adding further constraining equations (Ebner *et al.*, 2004). Specifically, the approach is to fit the matched HRSC points to the MOLA DTM. The HRSC points have to lie on a bilinear surface defined by four neighboring DTM grid points, which enclose the HRSC point. The distance of the HRSC point to the bilinear surface defined by the four points of MOLA DTM must be minimized. In addition to the collinearity Equation 1, one observation (Equation 5) is used for each HRSC point:

$$v_d + d = f(X_H, Y_H, Z_H, X_{M_i}, Y_{M_i}, Z_{M_i},)\ i = 1..4 \quad (5)$$

with three unknowns (X, Y, Z of HRSC tie point), one observation (difference d between HRSC point and MOLA surface) and twelve constants (X, Y, Z for all four MOLA DTM points) for each surface. The accuracy of the observed difference is determined by the accuracy of the MOLA points.

Results

The HRSC has obtained image strips from more than 140 orbits covering an area of approximately 22 million km^2 at the time of writing (October 2004). The bundle adjustment was evaluated with selected imagery from the Orbits 266, 279, and 292. Also, a block composed of these three strips has been analyzed. The strips were obtained in April 2004 from an orbit height between 265 and 297 km (note that the ground pixel size from an orbit height of 250 km is approximately 10 m). While the nadir channel was operated at full resolution, the stereo channels were operated with 2 × 2 pixel binning, reducing resolution to 20 m.

Figure 1 shows the results of matching for the three overlapping Orbits 266, 272, 292 and the distribution of the tie points. It can be seen that the tie points are evenly distributed over the whole block with a good connection between the strips. But, there are also some areas with a lower density of tie points due to low texture or image data gaps.

The next step is bias estimation. The *a priori* accuracy for the EO has been introduced into the bundle adjustment with a value of 1,000 m for the position and 0.025 degree for the attitude. The trajectory of the orbiter itself is considered to be stable which means its shape is fixed and not subject of the adjustment.

In a first evaluation, the ray forward intersections of the tie points are computed from the nominal values of the EO. Next, the bundle adjustment is carried out and the obtained ray intersections are compared. Note that for single strips only constant offsets (biases) of two out of three pointing angles, φ (pitch) and κ (yaw) can be determined. The translations and the pointing angle ω (roll) cannot be determined from the tie points alone. Within the block the three translations have been estimated for the two outer strips as well.

In Table 1 the accuracies of the object coordinates of the ray intersections are shown for the selected orbits and the block. The left value is the theoretical standard deviation of the ray intersections using the nominal EO. The right value shows the achieved standard deviations of the ray intersections after improving φ and κ (and all estimated biases for the block). The accuracies are in a range of about 5 m to 7 m in X (flight direction) and Y (across track). Z (height) accuracies of all orbits are about 11 m to 16 m. Obviously, the theoretical standard deviations of the ray intersections are improved by a factor of 2 to 3. Considering a ground pixel size of 25 m, this process translates to a final accuracy of about 0.4 pixel in X and Y and 0.8 pixel in Z.

Next, the HRSC object points have been tied to the MOLA DTM. This is realized by re-running the bundle adjustment with the additional constraints as described above and by estimating the biases (constant along the trajectory) of all six parameters of the EO (X_0, Y_0, Z_0, φ, ω, κ). In all cases the values can be determined with high significance, because the theoretical standard deviations of the bias values are lower than the bias values themselves.

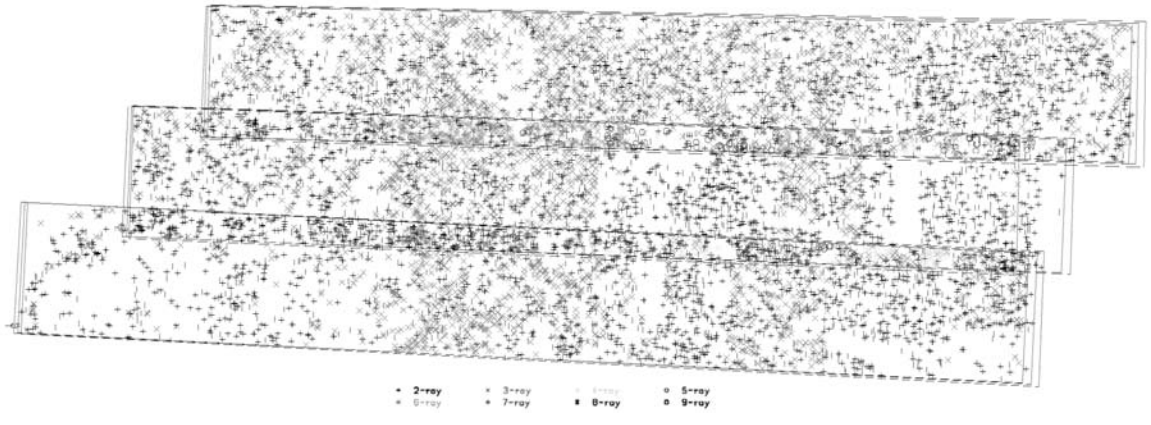

Figure 1. Distribution of tie points in the block of Orbits 266, 272, and 292 (north is to the right).

Table 1. Theoretical Standard Deviations of the Object Coordinates Before/After the Bundle Adjustment

Orbit	σX [m]	σY [m]	σZ [m]
266	11.7/4.5	18.7/5.1	39.2/11.0
279	17.0/5.3	10.5/4.4	35.3/11.2
292	10.6/4.9	16.5/6.2	35.3/13.8
Block	10.9/5.6	17.3/7.0	36.6/15.9

Additionally, the root-mean-square (RMS) difference in Z direction between object coordinates of the HRSC tie points and the MOLA DTM were studied. These differences are in the order of 200 m before and improved by a factor of 3 after the bundle adjustment. Therefore, there is a high consistency between HRSC points and the MOLA reference system after the bundle adjustment. This good agreement is clearly visible by comparing the differences graphically (Figure 2).

Finally, the theoretical standard deviations of the object coordinates for the three orbits and the block were checked and found to be less than 20 m, slightly larger than before (Table 1). This is explained by the fact that these accuracies are a combination of the accuracy within the orbit itself and the accuracies of the absolute orientation between orbit and MOLA DTM.

An Alternative Approach to Stereo Photogrammetric Processing of HRSC and SRC Images

The primary role of the U.S. Geological Survey (USGS), Flagstaff, Arizona on the HRSC team has been to help the team coordinate its efforts with the preexisting program of Mars cartography by supplying information about cartographic standards and control networks but, as data acquisition began it was deemed possible and desirable to develop an independent capability for stereo analysis of HRSC images at the USGS. The chosen approach, based on that previously taken with Mars Global Surveyor Mars Orbiter Camera (MGS MOC) images (Kirk *et al.*, 2003b), uses both the USGS digital cartographic system ISIS and the commercial off-the shelf (COTS) photogrammetric software SOCET SET® and exploits the strengths of each. The goals in applying this methodology to HRSC data were (a) to provide an independent check on the processing approaches used by the remainder of the team (described in the remainder of this paper and Scholten *et al.*, 2005); (b) to prepare for later systematic mapping with HRSC data at the USGS, given that the expected volume of imagery is likely to exceed the capacity of any single institution; (c) to bring the powerful ISIS tools for photometric modeling/correction photoclinometry (also known as shape-from-shading; Kirk *et al.*, 2003a) to bear on HRSC images; and (d) to implement a so-far unique capability for stereo processing of HRSC-SRC images.

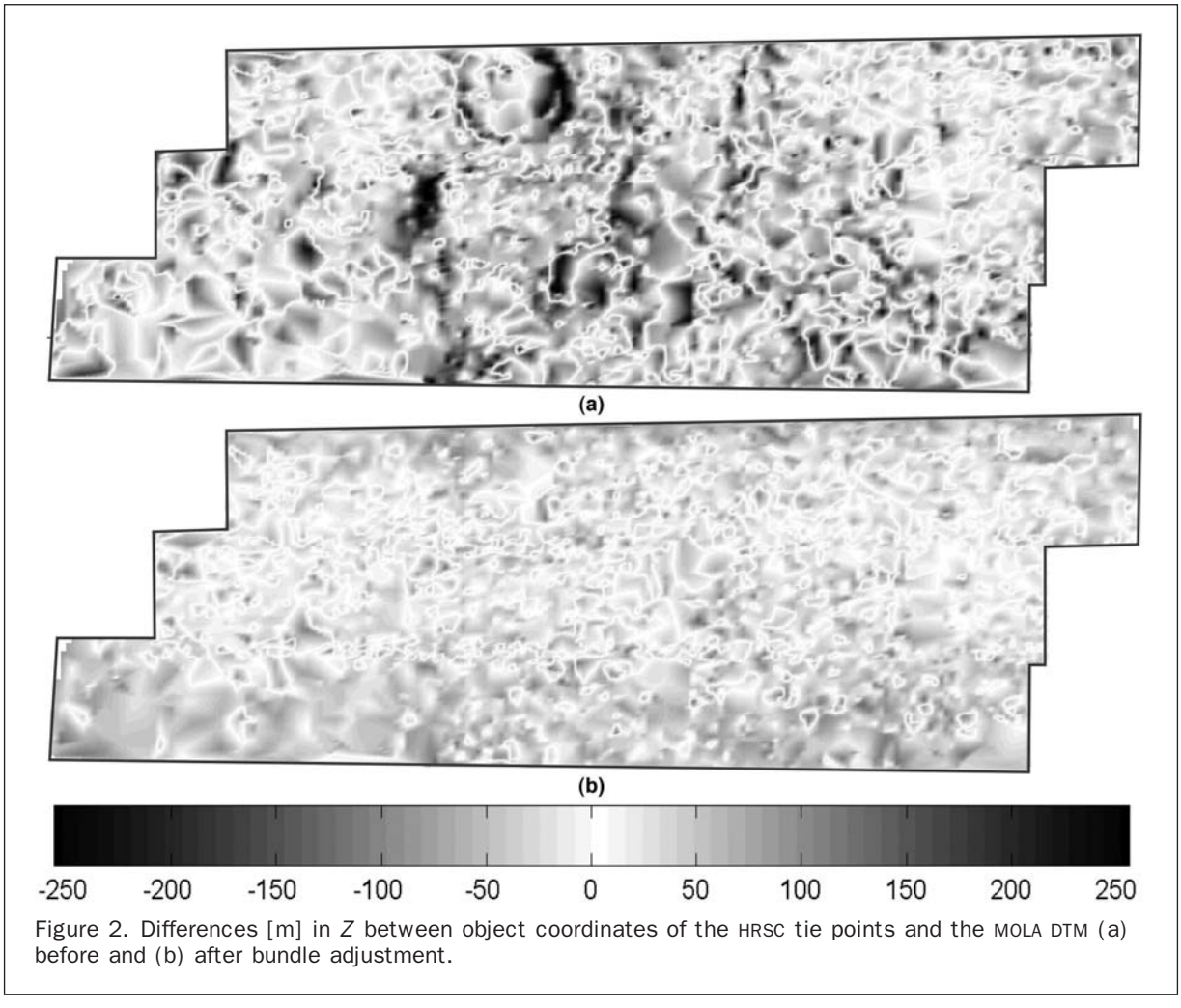

Figure 2. Differences [m] in Z between object coordinates of the HRSC tie points and the MOLA DTM (a) before and (b) after bundle adjustment.

The ISIS software (USGS Astrogeology Research Program, 2005) provides an end-to-end system for the analysis of digital images and production of maps from them that is readily extended to new missions. Its stereo capabilities are, however, limited. SOCET SET® (Miller and Walker, 1993; 1995) is tailored to aerial and Earth-orbital imagery, but provides a complete workflow with capabilities both for automated DTM production by hierarchical area-based matching and for quality control and editing of DTMs by using an optoelectronic stereo display and a 3D input device. Our processing approach for MOC and other stereo datasets has been to use ISIS to ingest images in an archival format, decompress them as necessary, and perform instrument-specific radiometric calibration. Software written in ISIS is then used to translate the image and, more importantly, orientation parameters and other metadata, to the formats understood by SOCET SET®. This commercial system is then used for "three-dimensional" processing: bundle-adjustment (including measurement of needed control points), DTM generation, and DTM editing. Final steps such as orthorectification and mosaicing of images can be performed with either system. This workflow was modified slightly for HRSC to take advantage of the standard processing performed at the DLR. We import the HRSC Level 2 (decompressed and radiometrically calibrated) data formatted in VICAR (Video Image Communication And Retrieval; see MIPL, 2005) into ISIS where it can immediately be used or exported to SOCET SET®. As part of the importation process the image data are reformatted to accommodate limitations of the ISIS and SOCET SET® sensor models. HRSC scanner images can have different exposure times for different lines, as recorded in VICAR line prefixes, but the sensor models require a fixed exposure time. Blocks of consecutive lines with constant exposure time are therefore identified and formatted as separate ISIS images. One line of overlap is provided between successive blocks so that they can be tied together during bundle adjustment. SRC images, which are provided in various cropped formats, are padded out to a fixed size corresponding to the full detector array.

The resulting image files can be modeled with the generic framing camera (for SRC) and pushbroom scanner (for HRSC) sensor models supplied with SOCET SET®, and with ISIS sensor models only slightly modified from those already implemented for similar sensors such as the Galileo SSI frame camera and MGS MOC line-scanner.

Both the DTM production and bundle-adjustment modules of SOCET SET® allow data from multiple sensors, including both framing cameras and scanners, to be analyzed jointly. This capability, unique in the HRSC team, offered the interesting prospect of generating extremely high resolution DTMs by combining SRC images with images of comparable resolution from the MOC Narrow Angle (NA) camera, which has an intrinsic pixel scale of 1.4 m but is most often operated in a pixel-summed mode with 3 m to 6 m resolution (Malin and Edgett, 2001). Neither instrument is designed specifically for stereo imaging as the HRSC is, but both are operated with off-nadir pointing at least part of the time. A manual search of the oblique SRC images (emission angle $e > 5°$) obtained during 13 of the first 413 MEX orbits revealed several sets overlapping MOC nadir imagery. A scientifically interesting example, located in the caldera of Olympus Mons, is shown in Figure 3. No difficulties were encountered in using the techniques developed for MOC-MOC stereo (Kirk *et al.*, 2003b) to bundle-adjust SRC frames h0037_0002–4 and MOC image E10–03979 to control provided by the Mars Orbiter Laser Altimeter and collect a DTM with 20 m post spacing and expected vertical precision (based on 0.2 pixel matching accuracy) <4 m.

HRSC scanner images can also be controlled and used to produce DTMs in SOCET SET®. Figure 4 shows an example

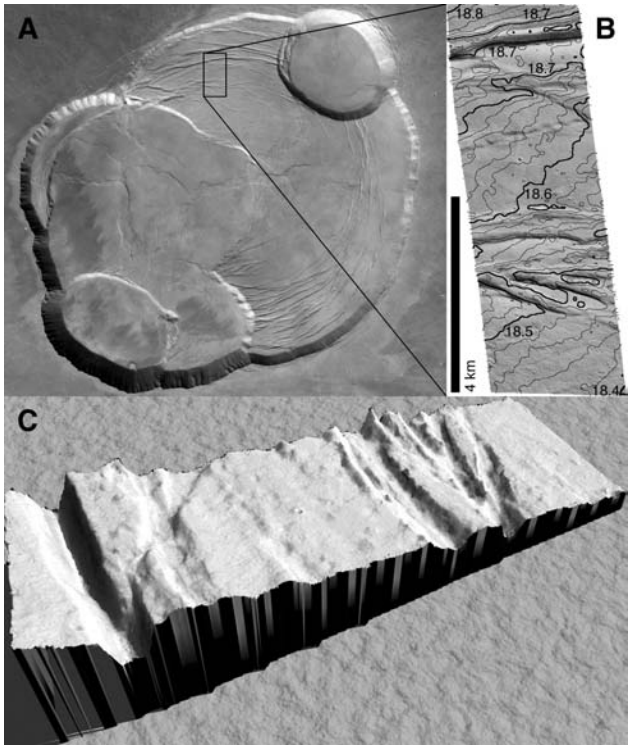

Figure 3. Example of joint stereoanalysis of HRSC-SRC (framing) and MGS MOC-NA (scanner) images in SOCET SET®, for an area within the summit caldera of Olympus Mons. (a) Context of the 75 km wide caldera produced by standard processing of HRSC data from Orbit 37. North is at top, resolution at approximately 12 m/pixel. (b) Orthomosaic of SRC frames h0037_0002–4 (resolution at 4.3 m/pixel, emission angle 31°) covering the outlined 2.8 × 8 km region of concentric fractures on the caldera floor. Elevation contours are derived from a DTM based on these images and MGS MOC-NA frame E10–03979 (resolution at 6.1 m, emission angle 18°). Contours are labeled in km above Mars reference surface; interval is 0.2 km. (c) Synthetic perspective view of SRC imagery draped on SRC-MOC DTM viewed from the northwest with vertical exaggeration of 4.

using images of the northwest flank of Olympus Mons obtained on Orbit 143. The results are preliminary, in the sense that manual editing of the smooth (low image texture) areas was required, but further experimentation to determine the optimal automatic-matching parameter values for HRSC images will likely reduce the need for such editing significantly in the future. This area is highly interesting scientifically because a localized area of the 7 km high scarp bounding the mountain appears distinct both morphologically (it has no distinct plateau edge) and materially (it appears brighter) than neighboring areas. A detailed DTM of the area can be used to photometrically normalize the images and quantify the apparent brightness of the area. Photometric modeling of the distinct surface units (Kirk *et al.*, 2004) can also provide information about both the intrinsic material properties of the surface, which relate to composition, and small (micron) scale textural properties, which may relate to processes of formation and modification. The HRSC intrinsically provides data for one approach to photometric modeling by imaging the surface at five

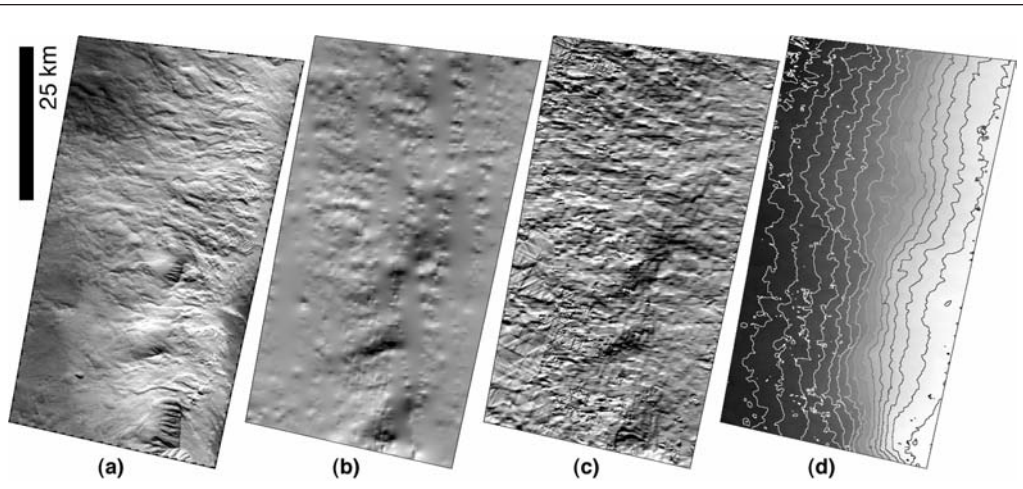

Figure 4. Example of DTM production from HRSC scanner data in SOCET SET®, for a portion of the northwest flank of Olympus Mons. (a) The HRSC nadir image h0143_0009 orthorectified at 25 m/pixel. The 38 × 76 km region shown covers part of the 7 km high basal scarp of the mountain. Considerable variability in albedo (brightness), texture, and morphology of the scarp are evident. (b) Synthetic image (shaded relief) computed from 512 m/post MOLA DTM. Illumination and assumed surface photometric properties match real image. Sparse sampling of altimeter tracks and even individual footprints are apparent. (c) Shaded relief computed from 100 m/post DTM derived from HRSC nadir/forward stereo image pair, same illumination as (b). Both fine-scale topographic details and DTM editing artifacts, particularly in smooth areas, are apparent. (d) Stereo DTM presented as grayscale image with contours. Elevation ranges from −1 km (black) to +7 km (white) with 0.5 km contour interval.

different phase angles with the broadband nadir, stereo, and photometric channels. Such images show significant variations in phase behavior related to both surface properties and the atmosphere in this area; special care is required in the analysis of atmospheric effects because the large elevation range results in a factor of 2 change in atmospheric column density across the scene. The strong phase effects also mean that accurate phase corrections are essential to reconstructing the HRSC color information. Modeling the incidence- and emission-angle variation of brightness at individual phase angles becomes possible given a high-resolution DTM and constrains the photometric properties in ways that strongly complement the phase-curve analysis. This kind of modeling only becomes possible with the HRSC stereo data, as the MOLA topography (Figure 5b) does not resolve the local relief (e.g., gullies) that is the object of photometric fitting.

Improvement of HRSC DTMs by Point Classification

Digital topographic models derived from HRSC images by area-based matching exhibit some deficiencies. The method's dependency on albedo features of the surface results in noisy or even pointless regions. Furthermore, point matching methods are not able to directly reconstruct linear structural features such as sharp terrain edges or crater rims. Therefore, the resulting surface models may show unnaturally rough areas caused by measurement noise, may have large gaps where image features are not detectable, and terrain discontinuities can appear smoothed. Figure 5a shows an orthophoto image and Figure 5b a shaded relief of a part of Hydraotes Chaos derived from points acquired by standard point matching (see Scholten *et al.*, 2005) in Orbit 18.

The approaches described in the following try to overcome these problems and to improve the quality and subsequently the interpretability of the final DTMs derived from HRSC images. The methods have been developed at the Institute of Photogrammetry and Remote Sensing at the Vienna University of Technology. The main ideas are aimed at eliminating the influence of the measurement noise by using point classification, bridging pointless areas with already available topographic information, and improving the modeling of linear structures with the help of structure line detection algorithm. Most of the described methods and algorithms are integrated in the Topographic Mars Information System (TMIS), a web-based application for management, analysis and visualization of Mars relevant topographic data. This system has been developed and realized during the MEX preparation phase (Dorninger, 2004).

Data

In addition to the randomly distributed points derived from HRSC images and provided by DLR, the track-wise organized MOLA points are used. Both data sets are available in Simple Cylindrical Map Projection. An automated method is used to detect and subsequently eliminate erroneous points of the MOLA data sets (released in July 2004) as described by Dorninger *et al.* (2004).

MOLA achieves an inner height accuracy of 1.4 m (Neumann *et al.* 2003). Thus, these points are well suited to serve as a first classification criterion for finding HRSC points within a certain tolerance band. Furthermore, MOLA is an active measurement system which is independent of surface structures or albedo features. Therefore, it provides points in regions where image matching fails due to missing features. Consequently, MOLA points can be used to bridge data gaps in the HRSC point set.

Method

The proposed and successfully applied method consists of several processing steps, commencing with the derivation of a distance map. The distance transformation, commonly

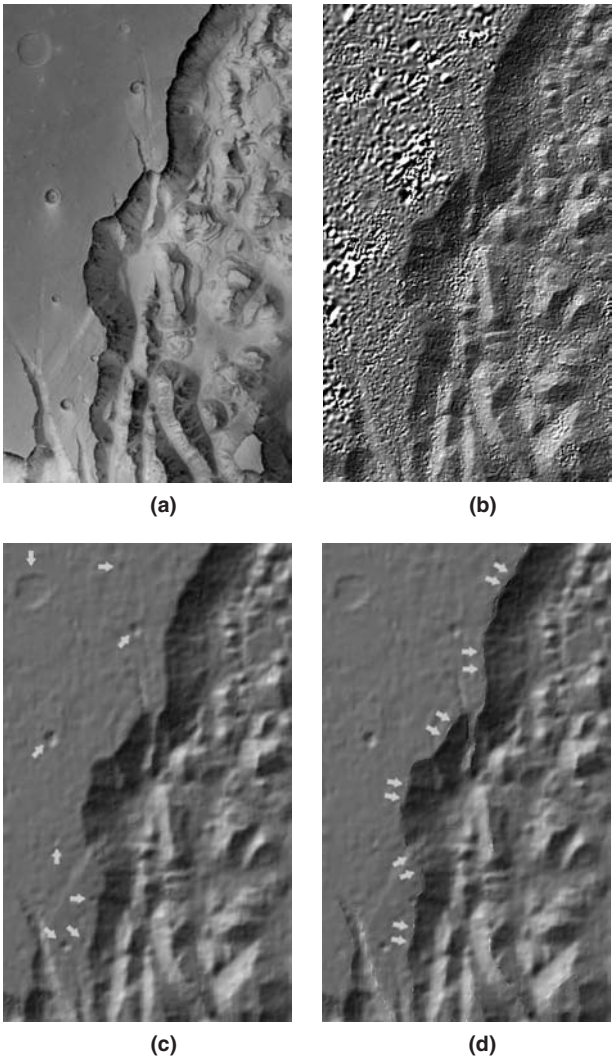

Figure 5. (a) Orthophoto image of test area (Orbit 18); (b) DTM derived from original HRSC points; (c) DTM derived from classified HRSC and all MOLA points (craters not detectable in Figure 6b become discernable and are marked by arrows); (d) Like (c) but with integrated breaklines (one breakline is marked by arrows; in the southern part of the figure there are several other breaklines).

referred to as *chamfering operation* (Borgefors, 1986), uses the MOLA points as input and results in a raster-based data set representing the distance from the available MOLA points. This chamfer image is used to define distance bands along MOLA tracks. In the area under investigation a maximum distance of ±400 m seemed to be appropriate with regard to the along track point spacing (300 m), thus leading to 800 m wide strips. The second step generates an intermediate DTM with a grid width of 250 m using all MOLA points within the distance band. Thereafter, a height tolerance above and below the intermediate DTM is used to classify, i.e., to include or sort out, the existing HRSC points. The magnitude of the tolerance depends on the *a priori* measurement accuracy and has been set to ±50 m in the presented example. During the third step a DTM is generated with all accepted HRSC and all MOLA points serving as a further intermediate DTM.

Thus, the preparation and initialization phase comprises the computation of a first distance band (±400 m) using chamfering and the determination of the first intermediate DTM (250 m grid width) derived from the given MOLA points within this band. Then, an iterative loop consisting of the following steps is started:

1. acceptance of HRSC points within a given height tolerance (±50 m) with respect to the intermediate DTM;
2. calculation of an intermediate DTM using all MOLA plus the accepted, i.e., positively classified, HRSC points within the currently valid distance band;
3. dilation of a distance band by a width of 100 m on either side;
4. calculation and subsequent integration of intermediary surfaces along the borders of the DTM derived in Step 2.

The iteration terminates as soon as all gaps could be closed or a certain termination criterion has been fulfilled. Details lost during the first coarse DTM derivation from the MOLA data can be recovered in the course of the following iterations when formerly rejected points are reaccepted. Eventually, a complete and uniform topographic model of the area of interest is created which integrates information acquired by HRSC and MOLA. Figure 6 shows the growing of the area covered by the DTM derived from accepted HRSC points after the first iteration steps.

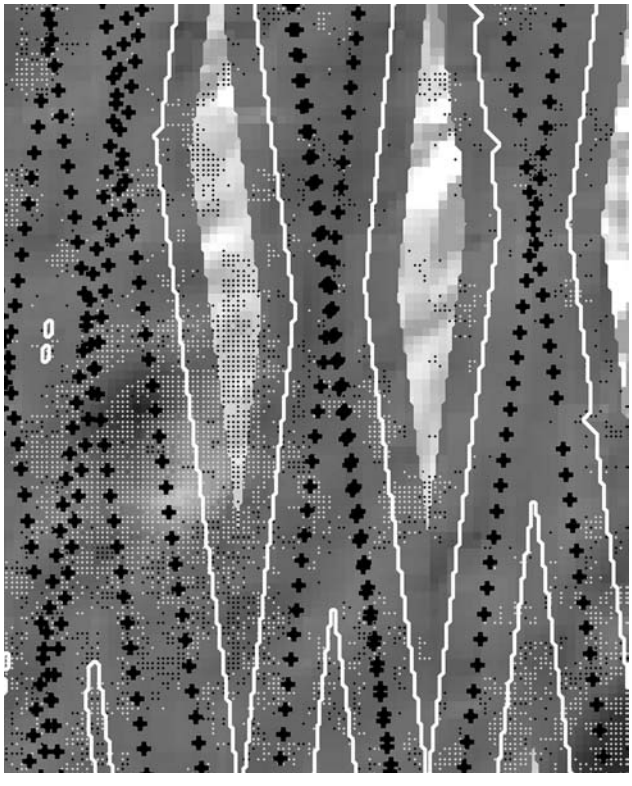

Figure 6. Intermediate result of HRSC point classification. MOLA points (black crosses) are used to define distance bands (white lines) and to derive a first DTM approximation which is used to accept HRSC points within a height tolerance band during the first iteration. The shading derived from accepted points appears smoother (dark gray area) than the not yet classified points (light gray). Accepted HRSC points are denoted in white, not (yet) accepted in black.

Results

In the test area, 82 percent of HRSC points are accepted using the parameters mentioned above. It has to be mentioned explicitly that the eventually accepted points have not been modified in any way, as the selection criterion is based on simple classification. This method is, therefore, independent of the subsequent DTM interpolation. TMIS uses the *Linear Prediction* (Kraus, 2000), also referred to as *Least Squares Interpolation* (Moritz and Sünkel, 1978), in order to generate a regular DTM grid from irregular point clouds. One of the advantages of Linear Prediction is the possibility to take into consideration the height noise of the input points, thus smoothing the surface with respect to a given or estimated *a priori* accuracy of the measurements. The *a posteriori* accuracy is determined by calculating the mean offset of the original points from the interpolated terrain model. It is a quality measure because it represents the actually achieved accuracy. In the current example the accuracy (RMS) yielded ±43 m before and ±24 m after classification deriving a DTM with a grid width of 100 m. Figure 5c shows a shading of the test area derived from the remaining HRSC and MOLA points after classification. Owing to the reduction of the measurement noise, surface features become discernible, which cannot be determined from the original point cloud. By comparing the shaded terrain with the corresponding part of an orthophoto image, the high quality of the DTM can be demonstrated (Figure 5a).

Current Work and Outlook

So far, only the point classification procedure has been developed and optimized for immediate DTM generation. No additional and auxiliary processes for the derivation of augmented information have been used yet. Therefore, current investigations and research activities aim at detecting and deriving three-dimensional breaklines from point clouds and at automatically integrating them into the DTM generation process. Breaklines are linear surface discontinuities which bear the potential for a significant improvement of the quality of the surface model. The method is based on a pairwise intersection of robustly estimated surface elements along the breakline (Briese, 2004). The test area contains sharp, linear discontinuities at the demolition of the upper, smooth highlands to the chaotic terrains. Figure 5d shows the capabilities of this method. This approach should be applicable for the modeling of crater rims, rift systems, or similar morphological structures.

The parameters used in the described classification and DTM generation process were determined empirically and may be optimal only for the area under investigation. Therefore, a verification is necessary in other areas (especially in those with quite different characteristics as, for instance, the southern hemisphere with its abundance of craters) in order to be able to set up a processing line for planet-wide applications with as little operator interaction as possible. In addition, investigations are also inevitable if data should be mosaiced whose quality is impaired by various external influences such as varying illumination conditions, atmospheric influences, or compression artifacts.

Densification of HRSC DTMs Using a Region-growing Adaptive Least-squares Correlator

The application of the matching approach developed at the University College London (UCL) is a contribution to further improvements of DTMs for Mars. The UCL 3D Image Maker was developed in the early 1990s (Day *et al.*, 1992) for the production of multi-image based DTMs employing Viking orbiter images with different resolutions and orientations. It is based on an adaptive least-squares correlation algorithm using region-growing in disparity space called "Gotcha" which employs seedpoints either generated randomly in an image pyramid or automatically using a feature detector. It was successfully applied to generate DTMs of several different areas on Mars (Thornhill *et al.*, 1993; Cook *et al.*, 1999) which were employed by geoscientists for studies of water flow on Mars.

The HRSC DTM routine production process was modified as shown in Figure 7 so that the output of the routine image matching could be employed as seedpoints for the Gotcha matcher, and the outputs of Gotcha were reconfigured so that the HRSC DTM production process could ingest them into the subsequent space intersection and transformation to planetographic/planetocentric coordinates above a reference ellipsoid or spheroid.

A 200 m DTM was derived by using the HRSC DTM matcher (Wewel, 1996) as a reference DTM for this study. Owing to the lack of contrast in certain areas, large image correlation windows frequently had to be employed. The HRSC DTM matcher was run on a nine-pixel grid over two different areas with very large changes in topography near the caldera (Orbit 37) and the western flank (Orbit 143) of Olympus Mons. The input images were pre-rectified using a global 5 km MOLA grid to an equal-area sinusoidal grid and re-sampled to the same maximum (nadir) pixel resolution. Gotcha then densified this nine-pixel grid to three-pixels using a 15-pixel radius as the patch size for the reasons of low signal-to-noise due to the lack of contrast within some of the scene.

Plate 1a shows a side-by-side view of the resultant Digital Disparity and Elevation Model (DDEM) for the reference grid (nine-pixel) and the Gotcha (three-pixel) grid. Figure 8 shows a similar side-by-side view, but this time of the hill-shaded DTMs derived from the DDEMs. It is self-evident that more DTM detail can be observed in the densified DTM. In fact, a slump feature (Figure 8 insert) can be observed in the Gotcha DTM which is missing in the reference DTM.

A quantitative inter-comparison of the resultant DTMs was performed using MOLA profiles but without performing a bundle adjustment. The profiles are shown in Figure 9 and the height difference statistics show that the RMS height accuracy for the two were 220.7 m (reference DTM) and 140.6 m RMS (Gotcha) with both DDEMs showing ray-ray intersection skewness of <50 m. The match coverage of the two different matchers for this area was 33 percent (reference DTM) versus 88 percent (Gotcha DTM).

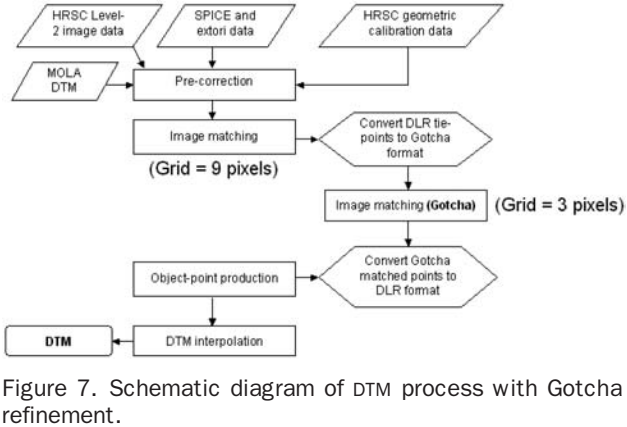

Figure 7. Schematic diagram of DTM process with Gotcha refinement.

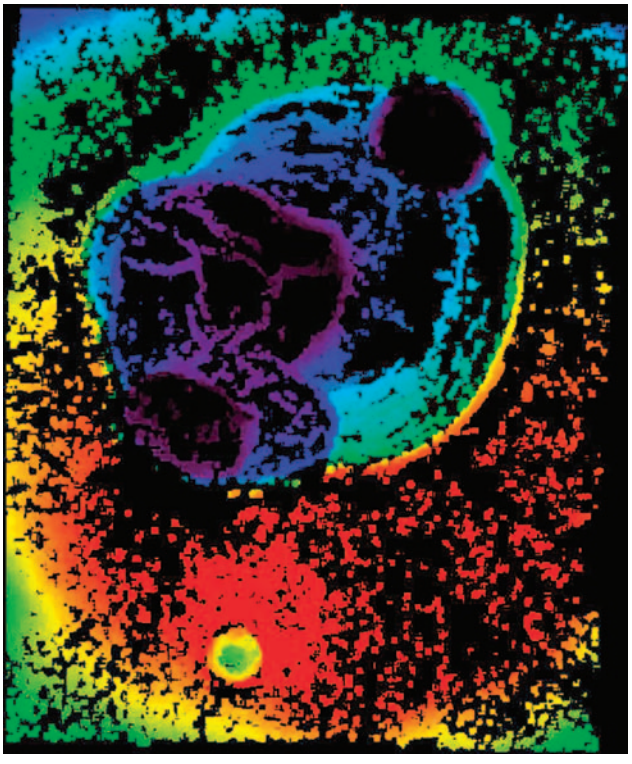

(a)

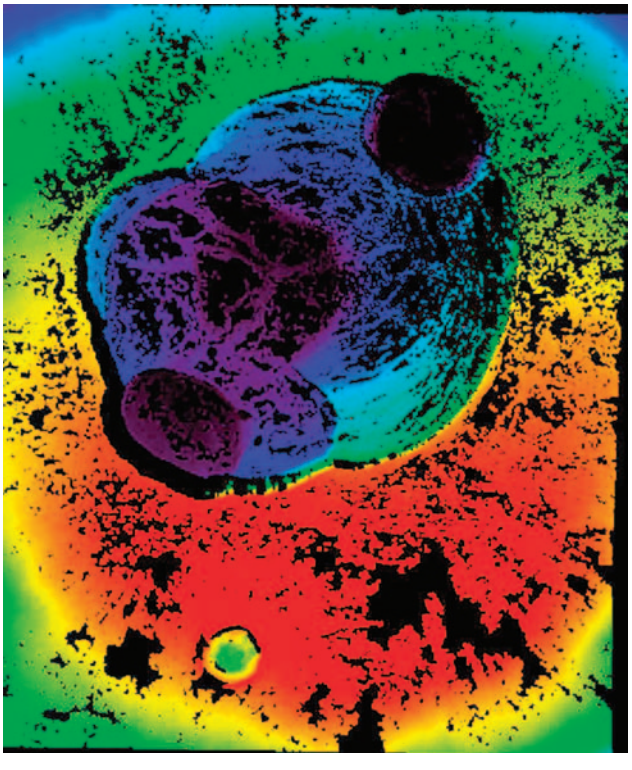

(b)

Plate 1. Intercomparison of (a) reference 3-pixel and (b) Gotcha 9-pixel grid matches converted to height (DDEMs) showing finer scale detail and better match coverage of the refined matcher.

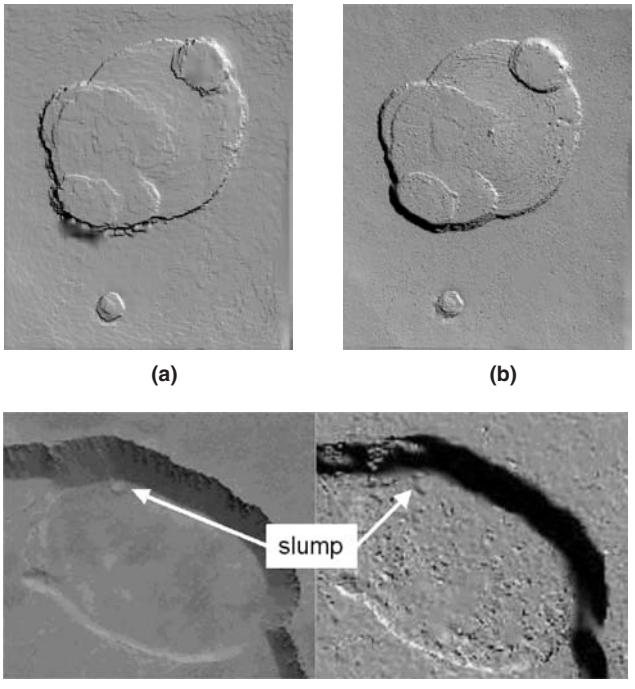

(a) (b) (c)

Figure 8. Hill-shaded DTM derived using reference DTM (a) based on DDEM in Plate 1a and Gotcha matcher (b); (c) shows a slump feature detected in the Gotcha DTM.

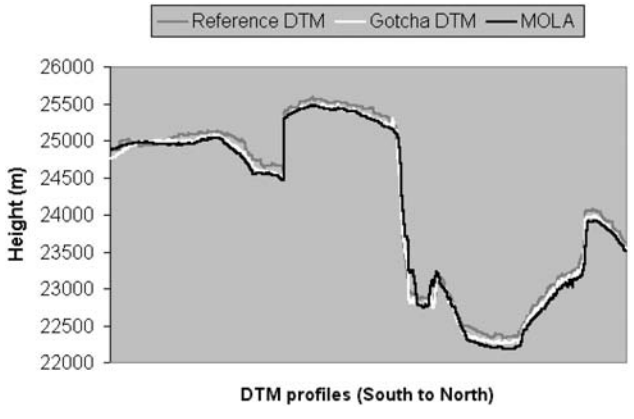

Figure 9. Profile intercomparison taken from reference DTMs, Gotcha with corresponding MOLA height profiles showing closer agreement between Gotcha and MOLA as well as overshoot problems with the MOLA profiles in certain locations.

De- and Re-Shading for DTM-Refinement and for Homogenization of Relief Shading

De-and Re-Shading (DRS) stands for a novel approach to complement and refine traditional digital photogrammetric and cartographic techniques. The main objective of DRS is both optimization and homogenization of the natural illumination-induced shades in image scenes. By artificially modifying the illumination (*Re-Shading*) not only uniform relief shading of mosaiced orthophoto images may be attained

(*Homogenization*), but also relief inversion effects caused by improper illumination direction can be eliminated (*Optimization*). Necessary and sufficient condition for reliable modifications of relief shading is a DTM with a precision closely related to the underlying image resolution. Improving the given initial DTM is a by-product of DRS. The final residual error level mainly depends on the fidelity of the DTM.

Many regions of the Martian surface display insufficient texture, structure or contrast required for precision photogrammetric image matching. The result is that object reconstruction may become weak, thus leading to erroneous, poorly resolved elevations. A particularly bad example is shown in Figures 10 and 11. In our studies, emphasis has been placed to complement photogrammetric Shape-from-Matching (SFM)-based object reconstruction by a Shape-from-Shading (SFS) approach, because one of the prerequisites of SFS, i.e., texture-less surface, is largely fulfilled. Widely known today in computer vision, SFS was introduced and defined thirty years ago by B.K.P. Horn, the "Father of SFS" (Horn, 1970). In fact, SFS as the *Deshading* kernel of DRS is capable of substantial refinement of the DEM obtained by stereo photogrammetry alone. Similar findings were already discussed by several authors (Dorrer *et al.*, 1998; Hashemi *et al.*, 2002; Rajabi *et al.*, 2003), yet never have been applied under real conditions and on a large scale. A somewhat more elaborate version of this treatise was discussed in Dorrer *et al.* (2004). The results so far demonstrate the potential of the method despite its present simplifications.

Figure 10. HRSC narrow-angle orthophoto image 15 km by 15 km.

Conception of De-Re-Shading (DRS)

The DRS process, developed at the Munich Bundeswehr University, is based on an elevation difference constrained comparison of the irradiance of an ortho-image (E) with the modeled radiance image (R) of the object scene. We assume that the ortho photo image was derived from an original HRSC image (I) together with the orientation and calibration state of the camera (C) during the time of exposure and an initial digital elevation model (Z) obtained by SFM.

Prerequisite for a definite solution is an initial DTM of sufficient quality. The stochastic model of the DTM may be given by the global elevation variance (Var Z) as elevation quality model (EQM). Other input parameters are the Bidirectional Reflectance Distribution Function (BRDF) and the sun vector (s). The present experimental version is restricted to constant BRDF, hence diffuse (Lambert) reflection, constant scene albedo, and elevation quality.

Shape from Shading (SFS)

Applied to real-world imagery, SFS is a non-trivial, generally ill-posed problem. SFS has been and still is treated largely as a mathematical exercise covering mostly small and limited problems. An excellent survey is given by Zhang *et al.* (1999). An important aspect concerns the coupling of deterministic and stochastic optimization approaches (Crouzil *et al.*, 2003) in order to determine optimal values for the penalty factors of the constraint terms.

From the methodical viewpoint, SFS may be defined as a constrained *Calculus of Variations* problem. Historically such constraints were predominantly incorporated to ensure convergence to a somewhat smoothed solution in order to make it manageable numerically and omit discontinuities (Horn, 1970). We believe, however, that due to the resolution

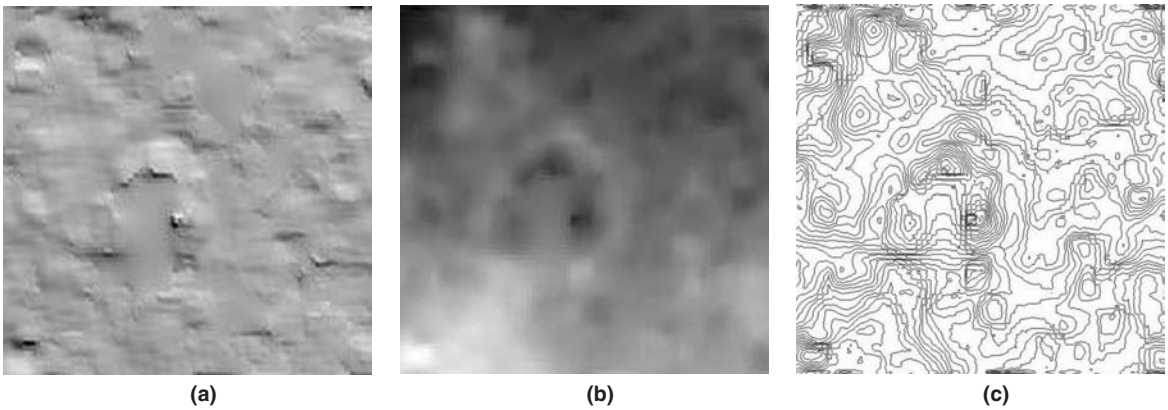

(a) (b) (c)

Figure 11. Initial DEM with derivative products prior to SFS. (a) Scene radiance, (b) DEM image, (c) Contour lines.

limit of pixel size, real discontinuities cannot exist in the discrete domain, hence smoothing regularization constraints become obsolete.

In our present SFS-approach, the basic (continuous) equation is defined by the minimization (or optimization) integral

$$J(Z) = \iint_{\Omega} \left[(E - \rho R)^2 + \lambda (Z - Z^{(0)})^2 \right] dXdY \longrightarrow min. \quad (6)$$

taken over a scene W in the (X,Y)-plane. Equation 6 is the unconstrained form of the constrained minimization functional, extended by the elevation constraint with l as a "penalty" factor. Z represents the surface of the desired DEM, $Z^{(0)}$ the initial DEM as approximation to $Z(X,Y)$ which is to be determined such that the functional $J(Z)$ becomes minimal. $R = R(p,q)$ as modeled reflected scene radiance is a function of the surface slopes $p = Z_X(X,Y)$ and $q = Z_Y(X,Y)$. Scene albedo factor and weight factor can be estimated by the expressions:

$$\rho = \iint ERdXdY / \iint R^2 dXdY \qquad and \qquad \lambda = (\sigma_E / \sigma_{Z^{(0)}})^2, \quad (7)$$

the latter representing the global stochastic model part (Crouzil *et al.*, 2003).

Instead of establishing the Euler-Lagrange equations associated with Equation 6 as, e.g., in Dorrer *et al.* (1998), and solve the discretized system of partial differential equations, we directly solve the discretized Equation 6 by variation of Z until the function J is minimized. By expressing the slopes simply as the convolutions of constant difference filters with Z, Equation 6 may now be solved iteratively by the method of conjugate gradients (CGM) (Shewchuck, 1994). The main advantages of CGM are that linearization of nonlinear functions is not required, convergence of the method normally is superlinear (Beckermann *et al.*, 2001), and Z will be determined indirectly. Some prerequisites for CGM such as convexity of J follow from $Z^{(0)}$ being rather close to Z.

Present Implementation

The present experimental version of the DRS software under development is a preliminary stand-alone version written in **C** and runs both under MS-Windows® and Linux. In addition, an independent APL2-version is used for testing and further evaluation purposes. The final **C**-version will be integrated into a comprehensive VICAR-based software package developed by the DLR Co-Investigator team. The limitations of the current rudimentary version of the DRS include: Lambert reflection, constant scene albedo factor, no shadows, no atmospheric correction, simplified stochastic DEM model, non-automated pre- and post-processing, rectangular scenes, and local Cartesian 3D system. Despite these limitations, the refinement of SFM-derived DTMs is remarkable.

Experimental Results

Figures 11 and 12 exhibit the main processing stages of a 150 pixel by 150 pixel subsection of an HRSC scene taken on 24 February 2004 at 266 km altitude in Orbit 143. Approximate location is 137° W longitude and 40° N latitude in the Acheron Fossae on the northern slopes of Olympus Mons. The topographic surface is generally inclined towards North. Illumination is somewhat from the south with 48° sun elevation. The initial orthophoto image (Figure 10) has been radiometrically enhanced for better detail perception. With 100 m pixel size the scene covers an area of 15 km by 15 km. The corresponding DTM is shown as a gray scale image in Figure 11b. It was generated by the DLR data processing group by image matching (SFM) from the HRSC stereo channels at the original 50 m resolution level. The area was intentionally selected as a first test site, since the quality of this SFM result (which should not be interpreted as the standard quality) demands for further refinement. The modeled scene radiance (Figure 11a) reveals enormous deficiencies in the DEM caused mainly by insufficient surface texture needed for SFM. Realize that Figure 11a should appear identical Figure 10 if the processing was error-free. The contour lines of the initial DTM (Plate 1b) may give an idea of the difficulties SFM has had for matching the image data.

Figures 12a, 12b, and 12c show the same scene after SFS-refinement with ten CGM-iterations. Despite some unwanted (and not yet understood) boundary effects visible mainly in the contour map (Figure 12c), the resulting scene radiance (Figure 12a) is more similar to the original orthophoto image (Figure 10). Although there are artifacts (probably illumination-induced) visible in the DTM-image (Figure 12b) and other errors due to incomplete modeling, a dramatic improvement of the SFM-derived photogrammetric DTM is obvious. A critical parameter is the optimal value for the weight factor. We processed the data with a series of different values. The one which intuitively and subjectively gave the most pleasing result was considered optimal (0.005). However, we do not (yet) understand its relationship with the underlying stochastic model as given by the right-hand relation in Equation 7.

The results presented are some of the outcomes of our first, yet most important development, i.e., fine-tuned shape

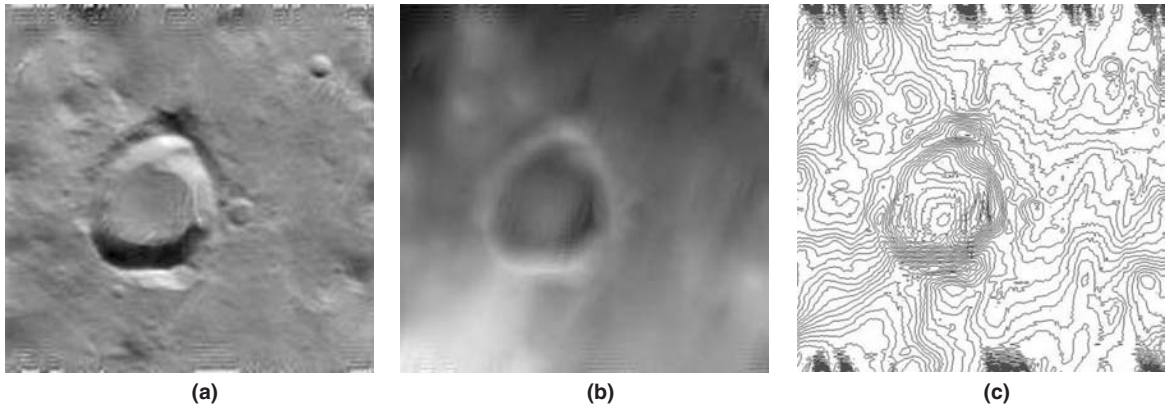

(a) (b) (c)

Figure 12. SFS-refined DEM with derivative products. (a) Scene radiance, (b) DEM image, (c) Contour lines.

from shading modeling of a given initial Martian surface DTM. Despite the preliminary stage of our studies, the results confirm the considerable refinement potential of SFS for an approximate DTM. In particular, after future removal of the main deficiencies in our approach (e.g., failure to comply with shadow extraction, space-variant stochastic elevation model, partial space-variant albedo), further stabilization and improvement for the DTM may be expected.

Generation of Topographic Maps

Based on HRSC imagery, large-scale topographic and thematic map products of the Martian surface are generated. The main task is the production of the Topographic Image Map Mars 1:200 000 series. As an innovation in extraterrestrial mapping, the production line has been designed as an entirely digital process using the cartographic software system Planetary Image Mapper (PIMap) which is developed at the Technical University of Berlin.

Cartographic Processing and Products

The standard map series within the Mars Express mission is the Topographic Image Map Mars 1:200 000 as described by Albertz *et al.* (2004). Moreover, the concept of this map series is the guideline for topographic mapping, i.e., for special target maps in larger scales, and the basis for thematic mapping purposes.

The latest definitions for Martian reference surfaces and coordinate systems have been adopted. Hence, map products are based on the rotational ellipsoid with an equatorial axis of 3,396.19 km and a polar axis of 3,376.20 km as defined by the International Astronomical Union (IAU) as the Mars IAU 2000 ellipsoid (Seidelmann *et al.*, 2002). The sheet lines follow the Martian standard coordinate system consisting of planetocentric latitudes and east longitudes (Duxbury *et al.*, 2002); the formerly used planetographic/west system is still shown as a second grid within the maps. An areoid, i.e., the Martian geoid, is defined as the topographic reference surface for heights (Smith, 2001).

Equal-area map projections are used for the new map series. The *Sinusoidal* projection is applied between 85° north and 85° south. However, polar map sheets, which cannot be mapped appropriately by this projection, are based on the Lambert Azimuthal projection (Albertz *et al.*, 2004). Altogether 10,372 maps cover all of Mars.

Map Generation with PIMap

The whole map production line is designed as an entirely digital process. Based on a detailed set of initialization parameters (ASCII file), this software generates and compiles the entire map content automatically. However, some interactive finalization is still necessary. PIMap is developed in C++ and runs under both Microsoft Windows® as well as Unix® and Linux environments.

Map sheets and derived products are based on HRSC color imagery, i.e., orthophoto mosaics; the topographic surface information of Mars is provided through DTMs. Both of these datasets are more or less routinely derived standard products of the photogrammetric processing, provided in VICAR format (Scholten *et al.*, 2005). For the integration into the particular map, an image is resampled (if necessary) and trimmed to the sheet lines within PIMap. Contour lines are derived from the DTM data and labeled respectively tickmarked automatically. PIMap also calculates different grids, which represent the coordinate systems defined for Mars (Duxbury *et al.*, 2002) and the map frame, accordingly. The mapped surface is completed by automatic placement of the names of Martian features and landing sites. Furthermore, map titles and the designations for planetary map sheets as well as additional information (including an index map showing the neighboring sheets of the map series) is generated.

With PDF, which is suited to handle both raster and vector data and thus the entire map content, a proven and widely used format is provided by PIMap. This is of importance, if a map sheet has to be finished interactively (e.g., with regard to the placement of feature names) using vector-oriented commercial software (Adobe Illustrator®, CorelDraw®, or Macromedia FreeHand®, respectively). Final products are then digital maps, which can be provided and/or printed on demand or introduced in geoinformation systems.

Since PIMap enables the computation of all common projections as well as the handling of different bodies (with spherical or ellipsoidal reference surfaces), it can be used for the generation of any type of planetary map. In comparison with common map generation procedures, this comprehensive approach is a substantial step towards future planetary cartography.

Cartographic Products

In preparation of the Mars Express mission, specimen sheets have been generated at the Technical University of Berlin (Gehrke *et al.*, 2003). Several special target maps making use of the first HRSC orthoimages and DTMs provided by DLR have been produced since early 2004 (see Albertz *et al.*, 2004).

An example of the standard map format is reproduced as Plate 2. With the ongoing systematic coverage of the Martian surface more and more image mosaics will be generated from overlapping image strips. Making use of such data, an increasing number of map sheets can be generated in the format of the Topographic Image Map Mars 1:200 000 series.

All of these mapping activities strongly follow the needs of other scientists, and are therefore well coordinated within the HRSC Co-Investigator team. Based on the results of such research, thematic map products, e.g., geologic maps, will also be generated.

Throughout several tests in preparation of the Mars Express mission and most important by generating the first map sheets from HRSC image data, PIMap has proven its operational status and has started a new era in digital planetary image map generation towards an entirely automatic process with very little interactive post-processing.

Conclusions

Although the HRSC experiment on Mars Express is just in its beginning phase, very promising results have already been achieved through the common efforts of the Photogrammetric/Cartographic Working Group within the HRSC Science Team. This success is very encouraging. Data of the quality, the systematic coverage, and the enormous potential for photogrammetric and mapping purposes, as provided by HRSC, will not be available from current or planned missions to Mars in the near future. Therefore, the working group members will make all possible attempts to further refine the procedures applied, and to achieve the highest accuracy for HRSC data products for the benefit of future Mars exploration.

Acknowledgments

The research projects described in this paper are part of the ESA Mission HRSC on Mars Express. The program is sponsored by the German Bundesministerium für Bildung und Forschung, the Austrian Space Agency (ASA), the NASA project Mars Express, and the UK Particle Physics and Astronomy Research Council (PPARC). The authors highly appreciate the co-operation in the international HRSC Science Team under the guidance of Principal Investigator Professor Dr. Gerhard Neukum (Freie Universität Berlin).

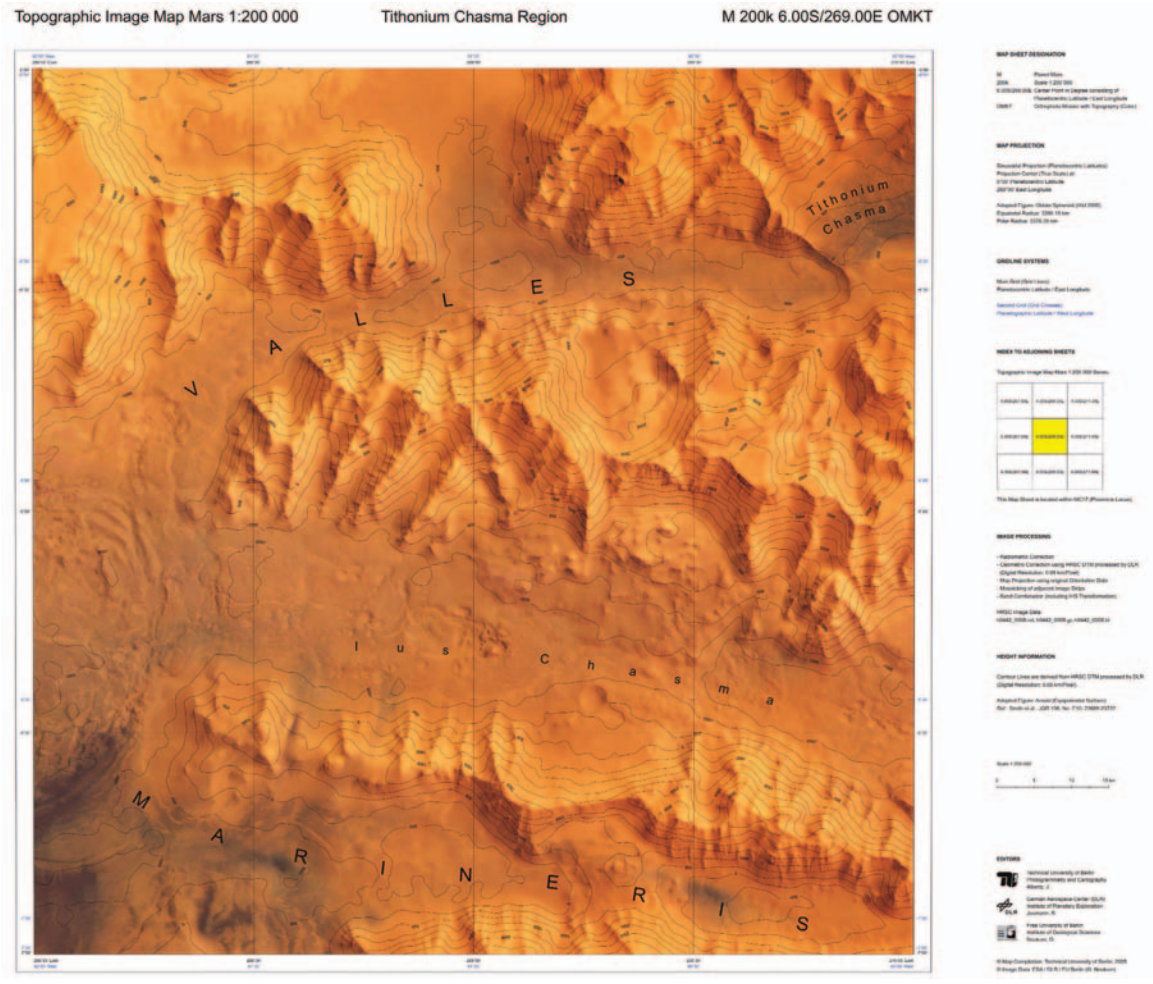

Plate 2. Topographic Image Map Mars 1:200 000, M 200k 6.00S/269.00E OMKT, "Tithonium Chasma Region" (Part of Valles Marineris).

References

Albertz, J., S. Gehrke, M. Wählisch, H. Lehmann, T. Schumacher, G. Neukum, and the HRSC Co-Investigator Team, 2004. Digital cartography with HRSC on Mars Express, *International Archives of Photogrammetry and Remote Sensing*, 35(B4):869–874.

Beckermann, B., and A.B.J. Kuijlaars, 2001. Superlinear convergence of conjugate gradients, *SIAM Journal of Numerical Analysis*, 39(1):300–239.

Borgefors, G., 1986. Distance transformation in digital images, *Computer Vision Graphics Image Processing*, 34(3):334–371.

Briese, Ch., 2004. Three dimensional modeling of breaklines from airborne laser scanning data, *International Archives of Photogrammetry and Remote Sensing*, 35(B3):1097–1102.

Cook, A.C., T. Day, and J.-P. Muller, 1999. ISPRS WG IV/5: Extraterrestrial Mapping Workshop: "Mapping of Mars 1999", 23–24 July. Caltech, Pasadena, California, URL: *http://wwwflag.wr.usgs.gov/USGSFlag/Space/Isprs/MEETINGS/Caltech99/abstracts/6170.pdf* (last day accessed: 13 July 2005).

Day, T., A.C. Cook, and J.-P. Muller, 1992. Automated digital topographic mapping technique for Mars, *International Archives of Photogrammetry and Remote Sensing*, 29(B4):801–808.

Crouzil, A., X. Descombes, and J.-D. Durou, 2003. A multiresolution approach for shape from shading coupling deterministic and stochastic optimization, *IEEE Transactions on Pattern Analysis and Machine Intelligence*, 25(11):1416–1421.

Dorninger, P., J. Jansa, and Ch. Briese, 2004. Visualization and topographical analysis of Mars surface, *Planetary Space Journal*, 52(1–3):249–257.

Dorninger, P., 2004. *A Topographic Mars Information System – Concepts for Management, Analysis and Visualization of Planet-wide Data*, Ph.D. dissertation, Institute of Photogrammetry and Remote Sensing, Vienna University of Technology.

Dorrer, E., and X. Zhou, 1998. Towards optimal relief representation from Mars imagery by combination of DEM and shape from shading, *International Archives of Photogrammetry and Remote Sensing*, 32(4):156–161.

Dorrer, E., H. Mayer, A. Ostrovskiy, S. Reznik, G. Neukum, and the HRSC Co-Investigator Team, 2004: De- and Re-Shading of Mars Express HRSC image data for homogenization of map relief shading, *International Archives of Photogrammetry and Remote Sensing*, 35(B4):1299–1303.

Ebner, H., W. Kornus, and T. Ohlhof, 1994. A simulation study on point determination for the MOMS-02/D2 space project using an extended functional model, *Geo-Informations-Systeme*, 7(1):11–16.

Ebner, H., M. Spiegel, A. Baumgartner, B. Giese, G. Neukum, and the HRSC Co-Investigator Team, 2004. Improving the exterior orientation of Mars Express HRSC imagery, *International Archives of Photogrammetry and Remote Sensing*, 35(B4):852–857.

Fischler, M.A., and R.C. Bolles, 1981. Random sample consensus: A paradigm for model fitting with applications to image analysis

and automated cartography, *Communications of the ACM*, 24(6):381–395.

Förstner, W., 1986. A feature based correspondence algorithm for image matching, *International Archives of Photogrammetry and Remote Sensing*, 26(B3/3):150–166.

Gehrke, S., M. Wählisch, H. Lehmann, T. Schumacher, and J. Albertz, 2003. Cartography with HRSC on Mars Express – A Specimen of the New Series "Topographic Image Map Mars 1:200,000", *Proceedings of the ISPRS WG IV/9 Extraterrestrial Mapping Workshop*, Houston.

Hashemi, L., A. Azizi, and M.H. Hashemi, 2002. Implementation of a single photo shape from shading method for the automatic STM Generation, *International Archives of Photogrammetry and Remote Sensing*, 34(B3):71–73.

Heipke, C., R. Schmidt, R. Brand, J. Oberst, G. Neukum, and the HRSC Co-Investigator Team, 2004. Performance of automatic tie point extraction using HRSC imagery of the Mars Express mission, *International Archives of Photogrammetry and Remote Sensing*, 35(B4):846–851.

Hofmann, O., P. Navé, and H. Ebner, 1982. DPS – A digital photogrammetric system for producing digital elevation models and orthophotos by means of linear array scanner imagery, *International Archives of Photogrammetry and Remote Sensing*, 24(B3): 216–227.

Horn, B.K.P, 1970. *Shape From Shading: A Method for Obtaining the Shape of a Smooth Opaque Object From One View*, Ph.D. dissertation, Department of Electrical Engineering, Massachusetts Institute of Technology, Cambridge, Massachusetts.

Kirk, R.L., J.M. Barrett, and L.A Soderblom, 2003a. Photoclinometry made simple . . . ?, ISPRS Working Group IV/9 Workshop "Advances in Planetary Mapping 2003", Houston, URL: *http://astrogeology.usgs.gov/Projects/ISPRS/Meetings/Houston2003/abstracts/Kirk_isprs_mar03.pdf* (last date accessed: 13 July 2005).

Kirk, R.L., E. Howington-Kraus, B. Redding, D. Galuszka, T.M. Hare, B.A. Archinal, L.A. Soderblom, and J.M. Barrett, 2003b. High-resolution topomapping of candidate MER landing sites with Mars Orbiter Camera Narrow-Angle images, *Journal of Geophysical Research*, 108(E12), 8088 (doi:10.1029/2003JE002131).

Kirk, R.L., E. Howington-Kraus, L.A. Soderblom, B. Giese, and J. Oberst, 2004. Comparison of USGS and DLR topographic models of Comet Borrelly and photometric applications, *Icarus*, 167, pp. 54–69 (doi:10.1016/j.icarus.2003.07.009).

Kraus, K., 2000. *Photogrammetrie Band 3, Topographische Informationssysteme*, 1st edition. Dümmler Verlag, Köln, pp. 154–180.

Malin, M.C., and K.S. Edgett, 2001. Mars Global Surveyor Mars Orbiter Camera: Interplanetary cruise through primary mission, *Journal of Geophysical Research*, 106(E10) 23, 429–23, 570.

Miller, S.B., and A.S. Walker, 1993. Further developments of Leica digital photogrammetric systems by Helava, *ACSM/ASPRS Annual Convention and Exposition Technical Papers*, 3, 256–263.

Miller, S.B., and A.S. Walker, 1995. Die Entwicklung der digitalen photogrammetrischen Systeme von Leica und Helava, *Zeitschrift für Photogrammetrie und Fernerkundung*, 63(1):4–16.

MIPL, 2005. Multimission Image Processing Laboratory: The VICAR Image Processing System, URL: *http://www-mipl.jpl.nasa.gov* (last date accessed: 13 July 2005).

Moritz, H., and H. Sünkel, 1978. *Approximation methods in geodesy*, Sammlung Wichmann, Neue Folge, Band 10, Wichmann-Verlag, Karlsruhe.

Müller, F., 1991. *Photogrammetrische Punktbestimmung mit Bilddaten digitaler Dreizeilenkameras*, Deutsche Geodätische Kommission, Reihe C, Nr. 372, München.

Neukum, G., R. Jaumann, and the HRSC Co-Investigator Team, 2004. HRSC: The High Resolution Stereo Camera of Mars Express, *ESA Special Publications* SP-1240.

Neumann, G.A., F.G. Lemoine, D.E. Smith, and M.T. Zuber, 2003. The Mars Obiter Laser Altimeter archive: Final precision experiment data record release and status of radiometry, *Lunar Planetary Science* XXXIV, Lunar and Planetary Institute, Houston.

Rajabi, M.A., and J.R.S. Blais, 2003. Optimization of DTM interpolation using shape from shading with single satellite imagery, *The Journal of Supercomputing*, 28:193–213.

Schmidt, R., and R. Brand, 2003. Automatic determination of tie points for HRSC on Mars Express, *ISPRS Workshop High Resolution Mapping from Space 2003*, 06–08 October, Hannover.

Scholten, F., K. Gwinner, T. Roatsch, K.-D. Matz, M. Wählisch, B. Giese, J. Oberst, R. Jaumann, and G. Neukum, 2005. Mars Express HRSC data processing – Methods and operational aspects, *Photogrammetric Engineering & Remote Sensing*, 71(10).

Seidelmann, P.K., V.K. Abalaki, M. Burs, M.E. Davies, C. de Bergh, J.H. Lieske, J. Oberst, J.L. Simon, E.M. Standish, P. Stooke, and P.C. Thomas, 2002. Report of the IAU/IAG working group on cartographic co-ordinates and rotational elements of the planets and satellites: 2000. *Celestial Mechanics and Dynamical Astronomy*, **82**, 83–110.

Shewchuck, J.R., 1994. An introduction to the conjugate gradient method without the agonizing pain, August, 54 pp., URL: *http://www-2.cs.cmu.edu/~jrs/jrspapers.html* (last date accessed: 13 July 2005).

Spiegel, M., A. Baumgartner, and H. Ebner, 2003. Orientation of Mars Express/HRSC imagery using laser altimeter data as control information, *ISPRS Workshop High Resolution Mapping from Space 2003*, 06–08 October, Hannover.

Thornhill, G.D., D.A. Rothery, J.B. Murray, A.C. Cook, T. Day, J.P. Muller, and J.C. Iliffe, 1993. Topography of Apollinaris-Patera and Maadim-Vallis – Automated extraction of digital elevation models, *Journal of Geophysical Research, Planets*, 98 (E12), 23581–23587

USGS Astrogeology Research Program, 2005. Integrated Software for Imagers and Spectrometers, URL: *http://isis.astrogeology.usgs.gov* (last date accessed: 13 July 2005).

Wewel, F., 1996. Determination of Conjugate Points of Stereoscopic Three Line Scanner Data of Mars96 Mission, *International Archives of Photogrammetry and Remote Sensing*, 31(B3): 936–939.

Wewel, F., F. Scholten, and K. Gwinner, 2000. High resolution stereo camera (HRSC) – Multispectral 3D-data acquisition and photogrammetric data processing, *Canadian Journal of Remote Sensing*, 26(5):466–474.

Zhang, R., T. Ping-Sing, J.E. Cryer, and M. Shah, 1999. Shape from Shading: A Survey, *IEEE Transactions on Pattern Analysis and Machine Intelligence*, 21(8):690–706.